Navigation of UAV using Phased Array Radio*

Sigurd M. Albrektsen[1], Atle Sægrov[2], Tor A. Johansen[1]

***Abstract*— Navigation and communication are two of the major challenges when flying unmanned aerial vehicles (UAVs) beyond visual line of sight (BVLOS), in particular when Global Navigation Satellite Systems (GNSS) are unavailable. The phased array radio system used in this paper aims to solve both communication and navigation with one system. To enable high efficiency data transfer, the radio system uses electronic beamforming to direct the energy from the ground radio towards the UAV, but to be able to do this, the ground radio needs to know the bearing and elevation angles towards the UAV. By measuring the round-trip time to compute the range and observing the direction of the incoming signal to compute the bearing and elevation angles, the phased array radio system is able to find the position of the UAV, relative to the ground radio, in all three dimensions.**

The phased array system is shown to provide absolute measurements for UAV navigation in radio line of sight, which can be used as a redundant system to GNSS measurements. By merging the radio measurements with barometer altitude data, a mean accuracy of approximately 24 m with a standard deviation of approximately 17 m compared to the real time kinematic (RTK) satellite navigation solution is achieved on a UAV flight at a distance of approximately 5 km.

I. Introduction

Today, two major challenges with unmanned aerial vehicle (UAV) flights beyond visual line of sight (BVLOS) are navigation and communication. UAVs' abilities to cover large distances in a short amount of time, and their maneuverability, make them valuable tools for many civilian tasks such as surveillance of power lines, search and rescue and scientific research. To be able to safely perform these tasks, however, an operator needs to know where the UAVs are, what they are sensing, and he or she needs to be able to send updated commands to the UAV.

When it comes to positioning sensors there are two main categories; absolute positioning systems, which measure a position in relation to a fixed point, and relative positioning systems, which measure a position in relation to the previous position. When using relative positioning sensors, the errors accumulate, as old estimates are added to the current estimate, and thus the accuracy of the estimated position will deteriorate over time. Conversely, an absolute positioning system will typically have bounded errors, and the errors will not vary over time as they are measured directly. The most commonly used absolute positioning systems today are global navigation satellite systems (GNSS) such as Global Positioning System (GPS), due to the low integration cost and global coverage.

There are, unfortunately, challenges when relying solely on GNSS positioning. Hardware failures, operation in areas with weak signal reception due to multipath or atmospheric effects, and malicious disruption of the signal through jamming [1], spoofing [2], selective availability (SA), or unintended electronic interference from other systems, makes it vital to have alternative sources of navigation. The state of the art solution to GPS-less navigation is using computer vision [3–10]. The main weakness of vision-based solutions is the need for visual features and such systems are therefore susceptible to both atmospheric and light conditions. When flying over a calm ocean there are also few visible features, even with high visibility. Another challenge with computer vision systems is that image analysis is both complex and computationally expensive. As the downlink data-rate from a UAV to the ground usually is too limited to transfer a high-quality video stream, especially on long-range flights, data analysis needs to be performed on-board. Due to the limited onboard computational power it is advantageous to reduce the computational power needed by the navigation system, to be able to focus on the mission specific tasks instead.

By using a phased array radio system (PARS), both the challenges of communication and navigation are addressed. By using electrical beamforming, the PARS is able to direct the energy from the transmitting antenna elements towards the receiving radio [11–14]. In addition to allowing efficient high-rate data transfer over long distances, the system is also able to provide positioning data. The position estimates are obtained by accurately timing the round-trip time of the signal and analyzing the direction of the incoming radio waves [15], [16]. This positioning system provides a local absolute position measurement, it is GNSS-independent and no complex signal analysis needs to be performed on board the UAV.

This paper studies a PARS as an alternative to GNSS-based positioning. As this system provides absolute position estimates, it is drift free and thus a valuable sensor for long duration flights. Due to a degradation in vertical accuracy, a solution of using a barometer as an altimeter to compensate for this is effect is proposed. The system is tested and verified

*This work was supported by the FRINATEK project "Low-Cost Integrated Navigation Systems Using Nonlinear Observer Theory" through the Norwegian Research Council (project number 221666), the MAROFF project "Autonomous Unmanned Aerial System as a Mobile Wireless Sensor Network for Environmental and Ice Monitoring in Arctic Marine Operations" (project number 235348), and the Centre of Autonomous Marine Operations and Systems (NTNU-AMOS) (project number 223254) at the Norwegian University of Science and Technology (NTNU).

[1]Sigurd M. Albrektsen and Tor A. Johansen are with the Centre for Autonomous Marine Operations and Systems (NTNU-AMOS), Department of Engineering Cybernetics, Norwegian University of Science and Technology (NTNU), Trondheim, Norway {sigurd.albrektsen,tor.arne.johansen}@ntnu.no

[2]Atle Sægrov is with Radionor Communications, Trondheim, Norway atle.saegrov@radionor.no

through a 35 min flight over the ocean and compared to a RTK (Real Time Kinematic) GPS solution.

This paper first gives an overview of the PARS used in Section II. Then an overview of the proposed UAV system, in which to use the PARS, is presented in Section III. A method of estimating the pose of the ground radio is given in Section IV. Experimental results from a flight with a UAV are then presented in Section V with results from radio measurements in Section V-A and barometer aided results, for handling vertical inaccuracies, in Section V-B. Section VI suggests future work and Section VII concludes the paper.

II. Phased Array Radio Navigation System

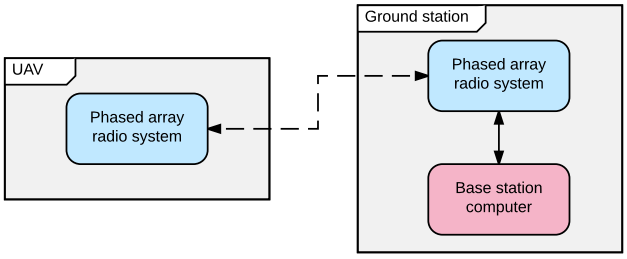

Fig. 1: A minimal overview of a UAV and ground station system. For clarity, the avionics are not shown.

The phased array radio system used is the Radionor CRE2-189 ground radio with a 8 by 8 grid of antenna elements, and an CRE2-144-LW with four antenna elements placed on the nose of the UAV. The onboard CRE2-144-LW has a weight of 85 g, dimensions of 120 mm x 65 mm x 13.3 mm. The CRE-144-LW is depicted in Fig. 2. To provide high efficiency data transfer from a ground station to a UAV, the PARS uses electrical beamforming to focus the transmitted energy in one direction. To properly be able to use beamforming, the ground radio needs to know the direction and preferably the distance to the UAV. To find this direction, the ground radio first sends an omnidirectional "ping"-signal, then observes the incoming response from the UAV radio, to find the direction towards UAV's antennas. The directional vector from the ground radio's antennas towards the UAV's radio antennas is calculated by observing how the signals are received by the different antenna elements on the ground radio. By using electrical beamforming to increase the performance of the radio system, a maximum user data throughput of 15 Mbps at 20 km, 7 Mbps at 30 km, and 2.3 Mbps at 60 km is achieved. An overview of the minimal system needed for position data is shown in Figure 1.

By accurately recording the time at which radio messages are sent from the ground radio and the time at which the corresponding wireless ACK-responses are received from the UAV radio, the round-trip time (RTT) of the signals are calculated by subtracting the internal computation time. This RTT is then used to calculate the distance between the ground radio and the UAV, knowing the speed of radio waves in air and the internal delays of the system. These direction and distance measurements then provide local absolute position measurements for the UAV, by knowing the pose of the ground radio.

Although the radio system does not have a global coverage, as opposed to GNSS, a sector of tens of kilometers can be covered from a single ground radio. The frustum covered by the ground radio spans 90° in both the horizontal direction and the vertical direction, with a maximal range of 60 km. Multiple ground radios can be used to ensure coverage of a larger operational area if needed. Note that the accuracy of the positional measurements in Cartesian coordinates will deteriorate proportionally with the measured distance, as the accuracy of the radio is specified as bearing and elevation angles from the ground radio.

As the PARS has a much higher signal-to-noise ratio (SNR) than GNSS signals transmitted from satellite orbit, jamming or spoofing the PARS position measurements are much more difficult. The PARS is also directional, as opposed to GNSS, and thus a malicious source needs to be in the visible sector of the ground radio to disrupt the position estimates. In addition, position estimates sent from the ground radio can be strongly encrypted to verify the sender's origin.

III. Experimental System Overview

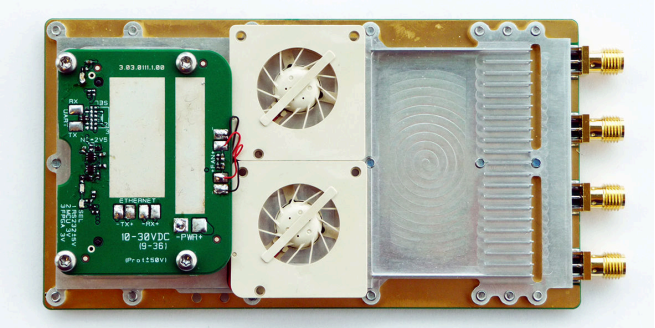

Fig. 2: The CRE2-144-LW phased array radio

As can be seen in Figure 3, the system on board the UAV is split in to three main parts; the avionics, the Experimental Navigation Stack, and the PARS. The avionics is responsible for the flight critical components of the UAV, and can operate without any other parts of the system during normal conditions. This system is based around the PIXHAWK[17] autopilot with a LEA-N7 GPS receiver [18], the PX4 Airspeed Sensor based on the MS4525DO sensor [19], and the standard integrated PIXHAWK sensor suite with IMUs[20–22] and a MEAS MS5611 barometer [23].

The Experimental Navigation Stack is responsible for providing a more accurate and robust navigation solution for the UAV using RTK GPS, a tactical grade IMU and a hardware synchronization board. To be able to calculate a high precision position solution based on GPS, raw satellite data with carrier-phase measurements are recorded on the base station. These measurements can either be transmitted from the ground station to the UAV, or be stored on the ground station and only be used for post-processing. A

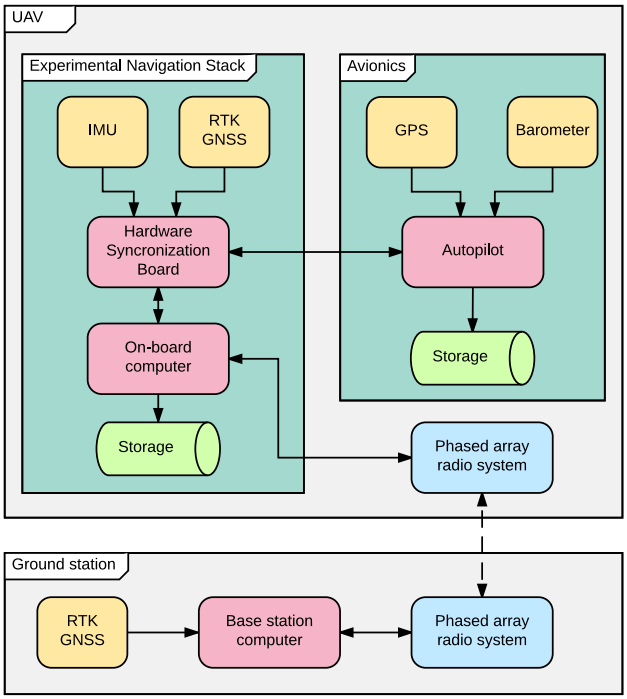

Fig. 3: Overview of the UAV and ground station systems used in experiments. The dashed line between the radios represents wireless communication. For simplicity, some components of the avionics are not shown in this overview.

separate GPS receiver, the ublox LEA M8T [24], is used due to the difficulties of relaying raw GPS measurements from the GPS receiver attached to the PIXHAWK.

To accurately synchronize the data a hardware synchronization board, the SyncBoard[25], is used to capture the PPS (pulse per second) signal from the GPS receiver and the time of validity (TOV) from the IMU, and attach accurate timestamps to the corresponding sensor messages. The data recorded by the SyncBoard is then transferred through USB to the ODROID-XU4 on-board computer and stored on the attached eMMC (embedded Multi-Media Controller) storage.

IV. Ground Radio Pose Estimation

Each time the ground radio is moved, its pose needs to be estimated. This can be done manually, by measuring the position using a GNSS receiver and the attitude using an inclinometer and a compass, but a more accurate, time efficient and elegant method is to estimate the pose automatically.

By accurately calculating the position of the UAV using real-time kinematic (RTK) satellite navigation, and accurately synchronizing the measurements from the ground radio measurements with the GPS clock, the radio-pose which would produce the observed measurements can be calculated. To compensate for noise and other inaccuracies of the measurements, several such measurement pairs are used. In [26], summarized by [27], this is done by taking the singular value decomposition (SVD) of the mean-subtracted measurements and then using the result to calculate the rotation matrix, $\boldsymbol{R}$, for the ground radio in the local East-North-Up (ENU) coordinate system.

First we convert the radio measurements, given in bearing, elevation and range, to Cartesian coordinates. Then we organize the measurements from the RTK solution and the radio measurements in two separate vectors.

$$\boldsymbol{p}_{\text{rtk}} = \begin{bmatrix} (x,y,z)_{1,\text{rtk}} \\ (x,y,z)_{2,\text{rtk}} \\ \vdots \\ (x,y,z)_{n,\text{rtk}} \end{bmatrix} \quad \boldsymbol{p}_{\text{radio}} = \begin{bmatrix} (x,y,z)_{1,\text{radio}} \\ (x,y,z)_{2,\text{radio}} \\ \vdots \\ (x,y,z)_{n,\text{radio}} \end{bmatrix} \tag{1}$$

Then we subtract the mean value of the measurements:

$$\boldsymbol{p}^*_{\text{rtk}} = \boldsymbol{p}_{\text{rtk}} - \bar{\boldsymbol{p}}_{\text{rtk}} \tag{2}$$

$$\boldsymbol{p}^*_{\text{radio}} = \boldsymbol{p}_{\text{radio}} - \bar{\boldsymbol{p}}_{\text{radio}} \tag{3}$$

and use the SVD as follows:

$$(\boldsymbol{p}^*_{\text{radio}})^\intercal \cdot \boldsymbol{p}^*_{\text{rtk}} = \boldsymbol{U}\boldsymbol{\Sigma}\boldsymbol{V}^\intercal \tag{4}$$

Then we calculate the rotation matrix as in Equation 25 in [27]. The $\det(\boldsymbol{V}\boldsymbol{U}^\intercal)$ term comes from the special orientation reflection case described in [27].

$$\boldsymbol{R} = \boldsymbol{V} \begin{pmatrix} 1 & & & \\ & \ddots & & \\ & & 1 & \\ & & & \det(\boldsymbol{V}\boldsymbol{U}^\intercal) \end{pmatrix} \boldsymbol{U}^\intercal \tag{5}$$

The position of the ground radio, $\boldsymbol{t}$, is then calculated by:

$$\boldsymbol{t} = \bar{\boldsymbol{p}}_{\text{rtk}} - \boldsymbol{R}\bar{\boldsymbol{p}}_{\text{radio}} \tag{6}$$

To achieve more accurate results, the measurements can be weighted based on the estimated accuracy from the sensors.

V. Experimental Results

To verify the positional measurements from the PARS, an experiment was carried out using a Skywalker X8 UAV at Agdenes outside Trondheim, Norway on June 23rd 2016 in good weather conditions and a forecasted wind of $15\,\text{km/h}$.

To validate the position measurements of the PARS, GPS measurements from the onboard uBlox LEA-M8T were used. To improve the accuracy of the GPS measurements, a base station was recording the signal from a fixed position, and an open source RTK solver, RTKLIB, was used to find the real time kinematic GPS solution. This solution is labeled RTK in the plots in this section. Note that the RTK solution is only used to calibrate the position of the PARS and for verification, but is not used to improve the radio measurements.

To ensure that the data for the ground-pose calibration is reliable, UAV missions can be preceded by a calibration step. To calibrate the ground radio pose, the UAV should be piloted in an area with good GPS coverage, while recording PARS measurements. This step can either be a separate flight, or the initial part of a longer mission. The recorded dataset can then be used in the calibration step described in Section IV.

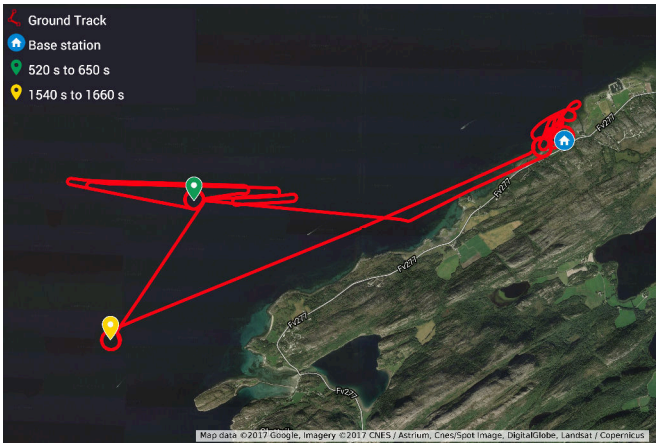

Fig. 4: A map of the flight track, with indicators showing the loitering circles from 520 s to 650 s and 1540 s to 1660 s after takeoff. The icon with the building indicates the base station.

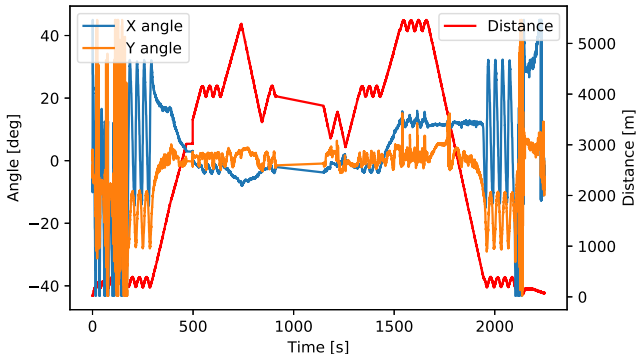

Fig. 5: Measurements from the phased array radio system

A. *Raw radio measurements*

Figure 5 shows the measurements from a complete UAV flight with a maximum measured distance of approximately $5\,\mathrm{km}$ from the ground station. When the UAV is close to the base station, from $0\,\mathrm{s}$ to $175\,\mathrm{s}$ after takeoff, the measured angle fluctuates as the UAV is outside the visible sector of the radio. Note that although the UAV maintains a fixed altitude, the angle measurement in the y-direction varies with approximately $4°$ at about $4125\,\mathrm{m}$. This is an inaccuracy likely due to reflections of the radio beams in the surface of the water, and results in an error of the position measurement from the radio of $4125\,\mathrm{m}\,\sin(4°) \approx 288\,\mathrm{m}$. Figure 6 shows a ground track of the flight from both the RTK GPS and radio measurements, with the radio position and opening frustum in the horizontal plane shown.

Figure 7 shows ENU plots from both the RTK GPS measurements, and Figure 8 shows zoomed-in views at times the UAV was loitering. In the *Horizontal* column of Table II the number of measurements in the horizontal plane within a specified accuracy are summarized. The error is calculated as the root-mean-square (RMS) of difference from the RTK position measurements.

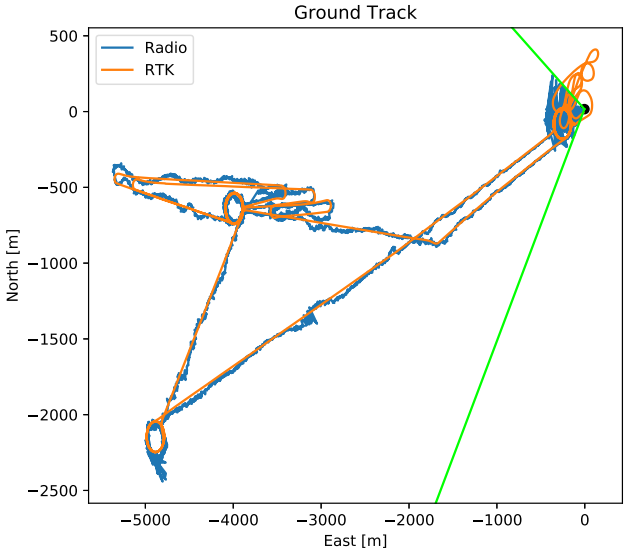

Fig. 6: Ground track of the PARS measurements and the RTK solution. The black circle marks the radio position, and the green lines indicate the visible frustum from the radio in the horizontal plane.

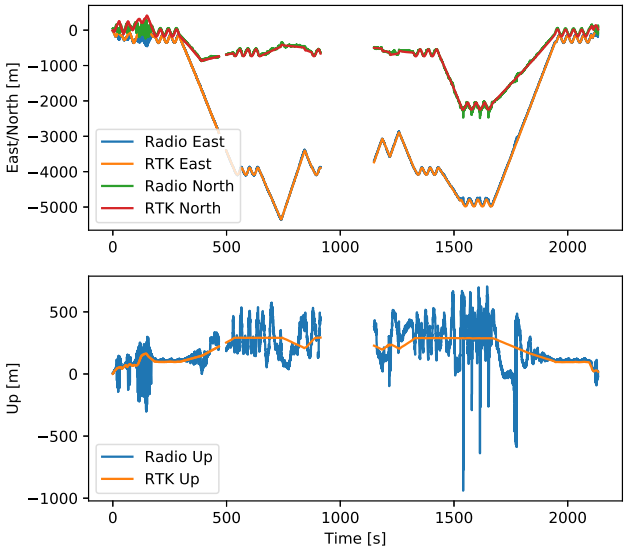

Fig. 7: Position measurements from the PARS, and RTK-GPS measurements for reference. The data from 897-901 s and 913-1148 s are missing due to a file transfer that disrupted the measurements.

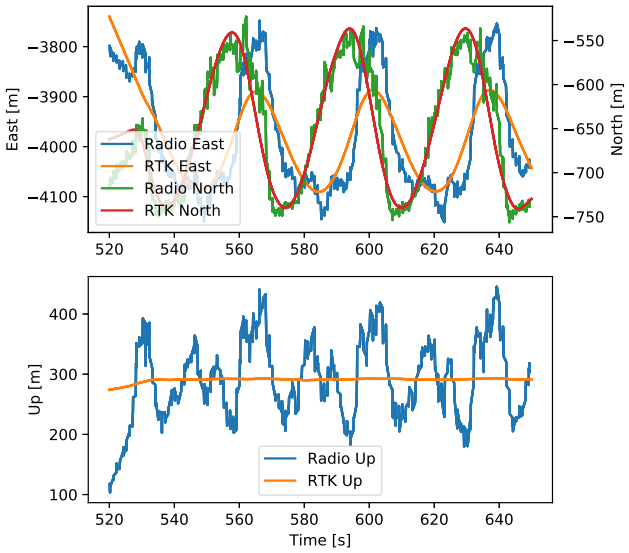

Fig. 8: PARS measurements from 520 s to 650 s of loitering UAV at a fixed altitude, and RTK-GPS measurements for reference

B. Barometric vertical correction

To compensate for the inaccuracies of the radio measurements in the vertical plane, measurements from the standard barometer (altimeter) connected to the PIXHAWK autopilot is used. As can be seen from Figure 9, these measurements are significantly closer to the RTK measurements than the radio measurements. Although the errors of a barometer are unbounded and vary with weather conditions, they tend to be considerably more stable than for example position estimates based on IMU, and should provide sufficiently accurate readings for the duration of a typical flight in most scenarios. A full plot of the combined data can be seen in Figure 9.

Table I lists these numbers in addition to the mean error and standard deviation of the error of both the radio-only and barometer supported measurements. Figure 10 contains a cumulative histogram of the RMS error and Table II lists example points from the histogram.

TABLE I: Comparison of radio-only and radio measurements compensated with barometer measurements

	Radio only	**Radio + barometer**
Mean error	96.22 m	24.23 m
Standard deviation	95.26 m	16.66 m

VI. Future Work

Although there are several benefits of using the absolute measurements from the PARS, such as being drift-free and having bounded errors, there are limitations as well. Similarly to GNSS, the PARS positioning system has a limited measurement rate and provides non-continuous measurements, which may lead to oscillations or other unwanted behaviors if used directly by an autopilot. To both increase the rate and provide smooth measurements an inertial measurement unit (IMU), which has a high measurement rate and indirectly provides continuous position measurements, can be used. As the IMU measurements are only accurate in short time intervals, fusing the absolute positioning measurements with the IMU data likely increases the accuracy and robustness of the estimates. This can for example be done using the extended Kalman filter (EKF).

To be able to rely on the radio measurements only, the vertical accuracy needs to be improved significantly. If we assume that the error in the vertical direction is due to reflections by the ocean surface, and that both the real

TABLE II: Percentage of measurements that are within a certain accuracy. The Horizontal measurements are radio-only measurements without the vertical components.

Measurements	**Horizontal**	**Radio only**	**Radio + barometer**
20.00 m	52.71 %	19.40 %	50.46 %
30.00 m	76.52 %	29.72 %	74.90 %
40.00 m	88.23 %	36.44 %	87.89 %
100.00 m	99.69 %	63.65 %	99.69 %
200.00 m	99.94 %	87.83 %	99.94 %

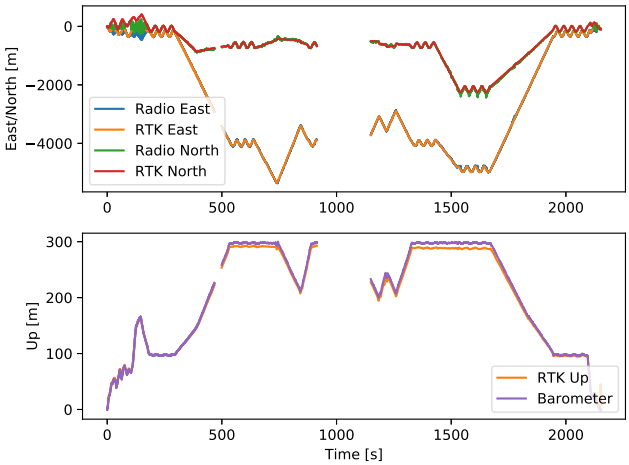

Fig. 9: RTK-GPS plotted against radio measurements in the horizontal plane and barometer readings in the vertical plane.

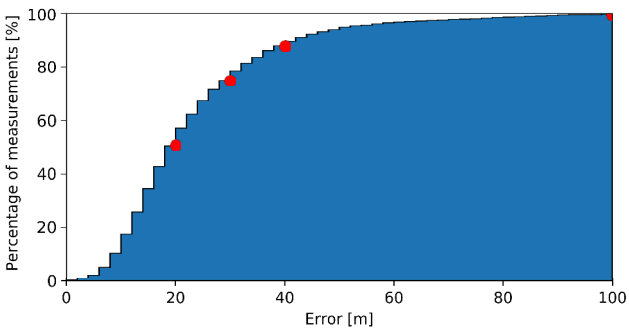

Fig. 10: Cumulative histogram of the root mean square of radio measurement errors in all three directions.

ranging signal and the reflected signals are detectable, the following approach can be used. If the detection algorithm is altered to provide one or more alternative measurements instead of only the strongest signal, we can prevent that the correct reading is discarded if the reflection has a stronger signal. If this is the case, techniques such as Multiple Hypothesis Tracking (MHT) can be used to make sure that the real signal is correctly tracked by the system. If this system is implemented, the system presented in this paper would no longer be reliant on the altimeter, and would provide a full absolute positioning system, independent of other measurements.

It would also be interesting to make a flight with multiple ground radios that observe the UAV from different positions on the ground. This would in theory not only improve the position estimates by having more independent readings, but also allow a larger area to be visible by the radios. This configuration will also allow us to verify the error sources of the radio system, such as reflections from the ocean surface. One might also imagine a hand-off scenario where when the UAV leaves a sector covered by one radio, the second radio provides the position estimates.

VII. Conclusion

In this paper we have studied a novel method of using a PARS and a barometer for absolute positioning of a UAV. As the phased array radio system is primarily used for communication, the system as a whole solves two major challenges with UAV operations. As radio beam reflections, caused by the ocean surface, disrupt the vertical accuracy of the position measurements of the UAV, a barometer is used as a vertical reference.

The PARS has been tested and verified with experimental results, and when combined with barometer readings, the mean error compared to RTK GPS is $24.23\,\mathrm{m}$ and $87.89\,\%$ of the measurements are within $40\,\mathrm{m}$ of the RTK GPS measurements. As the system provides absolute position measurements, independent from GNSS measurements, it is a valuable navigation source for BVLOS UAV flights.

Acknowledgement

The authors thank Tor Berg and Inge Aune Paulsen at Radionor Communications for their assistance, and our pilots Pål Kvaløy and Lars Semb at NTNU and Carl Erik Stephansen and Torbjørn Houge at Maritime Robotics. We are also thankful for the help in the construction and testing of the UAV payload provided by the rest of the UAV team at NTNU, in particular Jakob M. Hansen, Kasper T. Borup, Lorenzo Fusini, and Artur P. Zolich.

References

[1] A. Pinker and C. Smith, "Vulnerability of the GPS signal to jamming," *GPS Solutions*, vol. 3, no. 2, pp. 19–27, 1999.

[2] A. J. Kerns, D. P. Shepard, J. A. Bhatti, and T. E. Humphreys, "Unmanned aircraft capture and control via GPS spoofing," *Journal of Field Robotics*, vol. 31, no. 4, pp. 617–636, 2014.

[3] J. Hardy, J. Strader, J. N. Gross, Y. Gu, M. Keck, J. Douglas, and C. N. Taylor, "Unmanned aerial vehicle relative navigation in GPS denied environments," in *2016 IEEE/ION Position, Location and Navigation Symposium (PLANS)*, April 2016, pp. 344–352.

[4] A. Bachrach, S. Prentice, R. He, and N. Roy, "RANGE–robust autonomous navigation in GPS-denied environments," *Journal of Field Robotics*, vol. 28, no. 5, pp. 644–666, 2011.

[5] T. Krajník, M. Nitsche, S. Pedre, L. Přeučil, and M. E. Mejail, "A simple visual navigation system for an UAV," in *International Multi-Conference on Systems, Sygnals Devices*, March 2012, pp. 1–6.

[6] C. Liu, J. Nash, and S. Prior, "A low-cost vision-based unmanned aerial system for extremely low-light GPS-denied navigation and thermal imaging," *International Journal of Mechanical, Aerospace, Industrial, Mechatronic and Manufacturing Engineering*, vol. 9, no. 10, pp. 1750–1757, October 2015. [Online]. Available: https://eprints.soton.ac.uk/399629/

[7] S. Weiss, D. Scaramuzza, and R. Siegwart, "Monocular-SLAM–based navigation for autonomous micro helicopters in GPS-denied environments," *Journal of Field Robotics*, vol. 28, no. 6, pp. 854–874, 2011. [Online]. Available: http://dx.doi.org/10.1002/rob.20412

[8] S. Mishra and S. Saripalli, *GPS-free navigation for micro aerial vehicles*. American Helicopter Society International, 2015, pp. 189–193.

[9] L. Fusini, T. A. Johansen, and T. I. Fossen, "Dead reckoning of a fixed-wing UAV with inertial navigation aided by optical flow," in *2017 International Conference on Unmanned Aircraft Systems (ICUAS)*, June 2017, pp. 1520–1259.

[10] F. Kendoul and K. Nonami, "A visual navigation system for autonomous flight of micro air vehicles," in *2009 IEEE/RSJ International Conference on Intelligent Robots and Systems*, Oct 2009, pp. 3888–3893.

[11] G. M. Turner and C. Christodoulou, "FDTD analysis of phased array antennas," *IEEE Transactions on Antennas and Propagation*, vol. 47, no. 4, pp. 661–667, Apr 1999.

[12] D. T. McGrath, "Wideband arrays and polarization synthesis," in *2016 IEEE International Symposium on Phased Array Systems and Technology (PAST)*, Oct 2016, pp. 1–5.

[13] H. H. Vo, C. C. Chen, P. Hagan, and Y. Bayram, "A very low-profile UWB phased array antenna design for supporting wide angle beam steering," in *2016 IEEE International Symposium on Phased Array Systems and Technology (PAST)*, Oct 2016, pp. 1–8.

[14] N. Tsagkarakis, P. P. Markopoulos, and D. A. Pados, "Direction finding by complex L1-principal-component analysis," in *2015 IEEE 16th International Workshop on Signal Processing Advances in Wireless Communications (SPAWC)*, June 2015, pp. 475–479.

[15] P. Stoica and K. C. Sharman, "Maximum likelihood methods for direction-of-arrival estimation," *IEEE Transactions on Acoustics, Speech, and Signal Processing*, vol. 38, no. 7, pp. 1132–1143, Jul 1990.

[16] P. P. Markopoulos, N. Tsagkarakis, D. A. Pados, and G. N. Karystinos, "Direction-of-arrival estimation by l1-norm principal components," in *2016 IEEE International Symposium on Phased Array Systems and Technology (PAST)*, Oct 2016, pp. 1–6.

[17] L. Meier, P. Tanskanen, L. Heng, G. H. Lee, F. Fraundorfer, and M. Pollefeys, "PIXHAWK: A micro aerial vehicle design for autonomous flight using onboard computer vision," *Autonomous Robots*, vol. 33, no. 1, pp. 21–39, 2012.

[18] *NEO-7 u-blox 7 GNSS modules*, ublox, 11 2014, rev. R07.

[19] *MS4525DO*, Measurement Specialties, 7 2016.

[20] *L3GD20H MEMS motion sensor*, STMicroelectronics, 3 2013, rev. 2.

[21] *LSM303D 3D accelerometer and 3D magnetometer*, STMicroelectronics, 11 2013, rev. 2.

[22] *MPU-6000 and MPU-6050*, InvenSense, 8 2013, rev. 3.4.

[23] *MS5611-01BA03 Barometric Pressure Sensor*, Measurement Specialties, 9 2015.

[24] *NEO/LEA-M8T u-blox M8 concurrent GNSS timing modules*, ublox, 6 2016, rev. R03.

[25] S. M. Albrektsen and T. A. Johansen, "SyncBoard - a high accuracy sensor timing board for UAV payloads," in *2017 International Conference on Unmanned Aircraft Systems (ICUAS)*, June 2017, pp. 1706–1715.

[26] A. Horn, "Doubly stochastic matrices and the diagonal of a rotation matrix," *American Journal of Mathematics*, vol. 76, no. 3, pp. 620–630, 1954. [Online]. Available: http://www.jstor.org/stable/2372705

[27] O. Sorkine-Hornung and M. Rabinovich, "Least-squares rigid motion using SVD," Department of Computer Science, ETH Zurich, Jan 2017. [Online]. Available: https://igl.ethz.ch/projects/ARAP/svd_rot.pdf